Modulating Charge-Transfer Interactions in Topologically Different Porphyrin – C_{60} Dyads

Dirk M. Guldi,*[a] Andreas Hirsch,*[b] Michael Scheloske,[b] Elke Dietel,[b] Alessandro Troisi,[c] Francesco Zerbetto,*[c] and Maurizio Prato*[d]

Dedicated to Dr. Pedastur Neta on the occasion of his 65th birthday

Abstract: Control over the interchromophore separation, their angular relationship, and the spatial overlap of their electronic clouds in several **ZnP** – C_{60} dyads (**ZnP** = zinc porphyrin) is used to modulate the rates of intramolecular electron transfer. For the first time, a detailed analysis of the charge transfer absorption and emission spectra, time-dependent spectroscopic measurements, and molecular dynamics simulations prove quantitatively that the same two moieties can produce widely different electron-transfer regimes. This investigation also shows that the combination of **ZnP** and C_{60} consistently produces charge recombination in the inverted Marcus region, with reorganization energies that are remarkably low, regardless of the solvent polarity. The time constants of electron transfer range from the μs to the ps regime, the electronic couplings from a few tens to several hundreds of cm^{-1}, and the reorganization energies remain below 0.54 eV and can be as low as 0.16 eV.

Keywords: charge separation · charge transfer · electronic coupling · fullerenes · porphyrinoids · reorganization energy

Introduction

The composition, the interchromophore separation/angular relationship, the overall dynamic and stimulus-induced reorganization, and the electronic coupling are crucial factors in the development of charge transfer reaction centers.[1] Of particular interest are artificial model systems in which the introduction of simple molecular changes is used to control and tune the magnitude of the electron-transfer (ET) parameters. Typically, to ensure rapid, intramolecular ET processes, either in the form of energy or electron transduction, synthetic chemistry exploits the formation of covalent bonds[2] or the use of biomimetic methodologies, such as the formation of π-stacks, hydrogen bonds, van der Waals contacts, and so forth.[3] These and other effective strategies are borrowed from the organization principle of the bacterial photosynthetic reaction center[4] in which the electron-donor is basically a porphyrinoid moiety. Both the arrangement and respective orientation of the electron donor and acceptor are the result of the incorporation of light- and redox-active components into well-defined transmembrane proteins.

In the artificial models, the donor – acceptor link plays an essential role and is a potent means to restrain the electron-donor – acceptor couples in their positions.[1] Synthetic chemistry tools can be used to create the linkage and introduce a spacer between the donor and acceptor. Its effect is not limited to the structure, but also determines the size of the electronic coupling matrix element (V) between the fragments it separates, ideally the donor and acceptor. An important feature of a spacer is the possibility of introducing a systematic alteration of separation, orientation, and overlap without affecting the electronic nature of the donor – acceptor

[a] Dr. habil. D. M. Guldi
Radiation Laboratory, University of Notre Dame
Notre Dame, IN 46556 (USA)
Fax: (+1) 574-631-8068
E-mail: guldi.1@nd.edu

[b] Prof. Dr. A. Hirsch, Dipl. Chem. M. Scheloske, Dr. E. Dietel
Institut für Organische Chemie der Universität Erlangen-Nürnberg
Henkestrasse 42, 91054 Erlangen (Germany)
E-mail: hirsch@organik.uni-erlangen.de

[c] Prof. F. Zerbetto, Dr. A. Troisi
Dipartimento di Chimica "G. Ciamician"
Università degli Studi di Bologna
V. F. Selmi 2, 40126 Bologna (Italy)

[d] Prof. Dr. M. Prato
Dipartimento di Scienze Farmaceutiche
Università di Trieste, Piazzale Europa 1
34127 Trieste (Italy)
E-mail: prato@univ.trieste.it

Supporting information for this article is available on the WWW under http://www.chemeurj.org or from the author. Figure S1: top and side views of *trans-2*-**ZnP** – C_{60} (**2**), *meta*-**ZnP** – C_{60} (**4**) and *para*-**ZnP** – C_{60} (**1**); Figure S2: superposed structure of *meta*-**ZnP** – C_{60} (**4**); Figure S3: details regarding the determination of the thermodynamic parameters.

DOI: 10.1002/chem.200304995

pair, whereby the coupling is proportional to the overlap of their electronic clouds. In other words, the exponential decay with the distance of the coupling may be modified by contributions from an intervening medium, for example, solvent.

After the donor and the spacer(s), suitable acceptors need to be identified. Fullerenes have proved to be a rich platform on which to conduct charge-separation (CS) studies.[5–13] These three-dimensional building blocks are now readily available and exhibit three characteristics of great relevance for ET reactions:

1) Fullerenes are extremely good electron acceptors.[14]
2) Fullerenes undergo multiple derivatization processes and can form a number of isomers in which two hexagon–hexagon edges have reacted to provide the attachment point for other molecules to be tethered.[15]
3) Primarily because of its rigid structure, fullerenes possess a remarkably low reorganization energy upon ET reactions.[16] A small reorganization energy is one of the key-factors in decreasing energy waste. In general, two-dimensional electron acceptors have much larger reorganization energies. The small reorganization energy of $\mathbf{C_{60}}$ renders it an extremely useful building block for exploring the modulation of rates and yields of charge separation (CS)/charge recombination (CR), for which conventional electron acceptors, such as quinones, have proved unsatisfactory.

It is notable that despite the number of synthetic model systems so far investigated,[10a, 17] the detailed description of geometrical factors that govern ET has remained unclear. In this paper, we compare the effects that arise from structurally different donor–acceptor topologies and demonstrate that the variation of distance and mutual orientation of a linked zinc tetraphenylporphyrin (**ZnP**) and fullerene ($\mathbf{C_{60}}$) reactant pair affects the charge-transfer (CT) parameters. The simplest way to alter the relative orientation of a two-dimensional planar electron donor (**ZnP**) with respect to a three-dimensional spherical electron acceptor ($\mathbf{C_{60}}$) is through synthetic modifications that are now available. An important issue, in this context, is the intramolecular flexibility and the associated variation of distance and orientation that can occur on a timescale comparable or faster than ET. Here, a combination of molecular dynamics and quantum chemical calculations is used to estimate these "fast-factors" as a function of the solvent. Despite different absolute rate constants for the forward and backward ET processes, which reflect the degree of interactions in the ground state and in the excited state, all systems reveal a fundamental common feature: the charge recombination kinetics are consistently located in the inverted region of the "Marcus parabola".

Results and Discussion

Synthesis and structural modeling: The synthesis and structural characterization of the dyads **1**,[18a] **2**,[18b,c] and **3**[18d] has been described previously. They were prepared by one- or twofold cyclopropanation of C_{60} and the corresponding bismalonates.[18] The synthesis of the new dyad **4** is summarized in Scheme 1. The precursor malonate **5** was synthesized via the substituted 3-hydroxybenzaldehyde **6**, with a malonate terminus. The co-condensation of **6** with benzaldehyde and pyrrole under Lindsey conditions[19] with Ph_4PCl and $BF_3 \cdot Et_2O$ as a catalyst in CH_2Cl_2 afforded the porphyrin precursor **7**, which was subsequently metallated with $Zn(OAc)_2$ to give porphyrin malonate **5**. This compound was fully characterized by a variety of techniques: ^{1}H NMR, ^{13}C NMR, and UV-visible spectroscopy and fast-atom bombardment mass spectrometry (FAB-MS). Finally, Bingel cyclopropanation of **5** with C_{60} led to the formation of the dyad **4**.

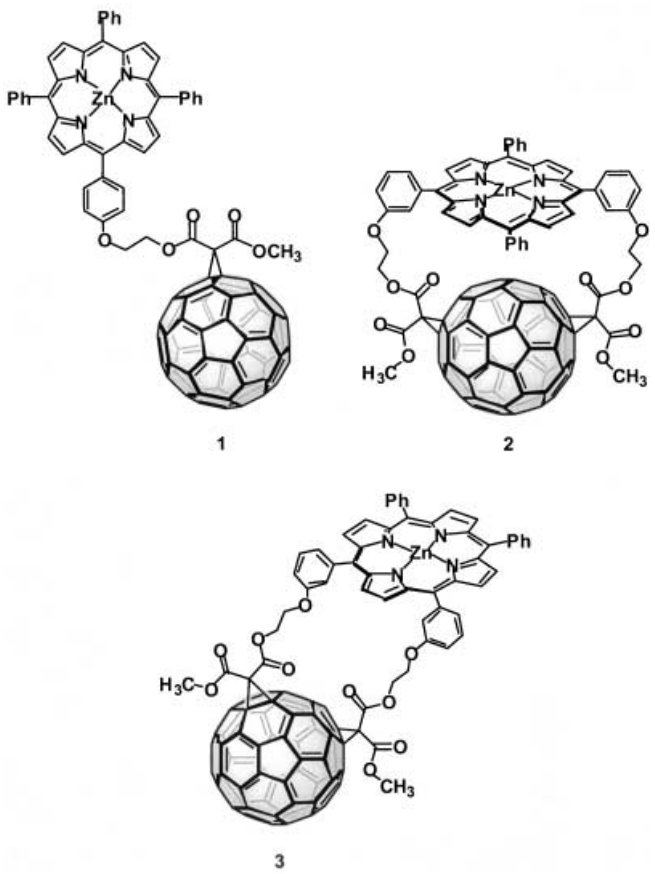

First, the singly linked porphyrin–fullerene ensembles shall be discussed. In the two ensembles, the substitution pattern of the phenyl groups of the porphyrin differs, that is they are either *meta*- or *para*-linked. This imposes a notable impact on the mutual orientation of porphyrin and fullerene. In particular, the *para*-substituted porphyrin system (**1**) is expected to furnish closer contacts but poorer overlap with the fullerene than the *meta*-analogue (**4**), because of steric constraints. For top- and side-view illustrations see the Supporting Information (S1). Despite the flexibility of the ethylene bridge, molecular modeling leads to the conclusion that the upper part of the cage of the fullerene is covered by the porphyrin (see Supporting Information (S2)).

To introduce more rigid packing into the porphyrin–fullerene ensembles, a double-linkage was pursued.[20, 21] Modeling of doubly linked porphyrin–fullerene dyads suggests the use of *meta*- rather than *para*-substituted adducts.

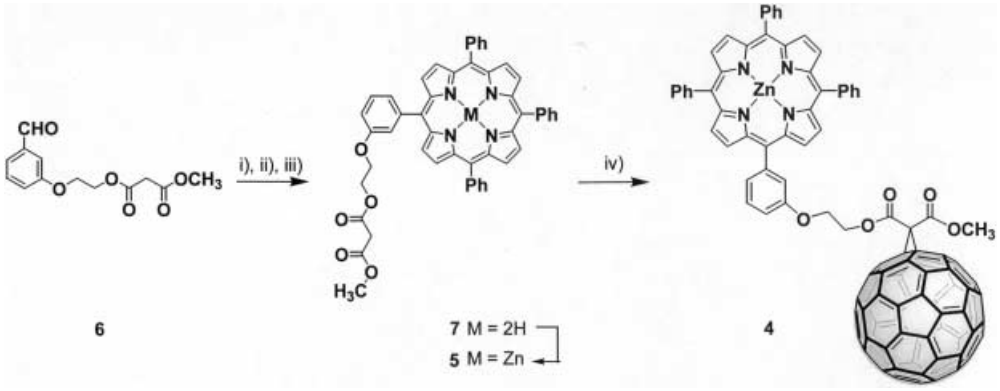

Scheme 1. Synthesis of the mono-linked **4**: i) benzaldehyde, pyrrole, Ph_4PCl, BF_3*Et_2O, CH_2Cl_2, RT; ii) *p*-chloranil, reflux, (silicagel, CH_2Cl_2/EtOAc (20:1)); iii) $Zn(OAc)_2 \cdot 2H_2O$, THF, reflux; iv) C_{60}, DBU, toluene.

The dyads *trans*-2-**ZnP – C$_{60}$** (**2**) and equatorial-**ZnP – C$_{60}$** (**3**) were modeled by using MM+ force field.[22] The results are shown in Figures 1 and 2, respectively. Molecular dynamics calculations of six randomly selected conformers of both of these dyads showed that:

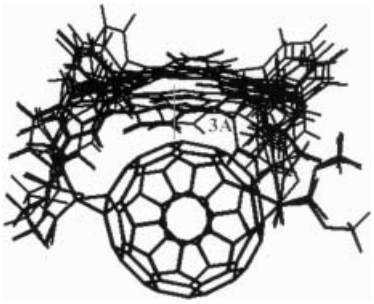

Figure 1. Superimposed conformers of dyad **2**.

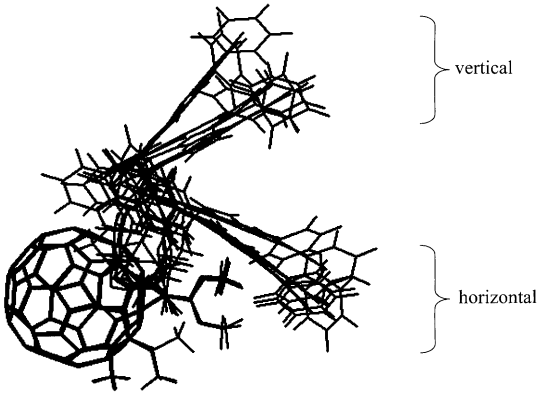

Figure 2. Superimposed conformers of dyad **3**.

1) Due to the double linkage, the variability of relative orientation of the two chromophores within each dyad is very limited. There is very little conformational space accessible. In **2**, the face-to-face alignment is completely locked, while in **3** only two types of face-to-edge orientations (vertical and horizontal) were found. NOE measurements revealed, however, that the horizontal conformation has a very low population (0.2%) relative to the vertical one (99.8%). Both systems therefore possess strong rigidity.
2) The face-to-face alignment in **2** with the shortest interplanar distance (Zn–C: 3 Å) leads to appreciable π – π stacking, whereas the face-to-edge alignment in **3** prohibits effective π – π interaction. The resulting distances (Table 1) suggest that one has to consider the product of distance and overlap to assess the interaction between porphyrin and fullerene. It can also be noted that close separation but little overlap can be compensated by good overlap and larger distances—compare, for example, *para*-**ZnP – C$_{60}$** (**1**) and *meta*-**ZnP – C$_{60}$** (**4**) (Supporting Information S1).
3) Dyad **3** can accommodate a solvent molecule, such as toluene, between the two moieties.

Table 1. Ground-state absorption maxima and their extinction coefficients of different **ZnP – C$_{60}$** donor – acceptor ensembles in CH_2Cl_2 at room temperature.

	2	**4**	**3**	*meta*-**ZnP**	**1**	*para*-**ZnP**
R_{ee} [Å][a]	3.0[b]	5.86	6.18		3.23	
Soret-band	429 (5.44)	427 (5.44)	425 (5.46)	421 (5.76)	418 (5.63)	420 (5.66)
Q-bands	552 (4.21)	551 (4.29)	549 (4.26)	548 (4.34)	548 (4.24)	549 (4.50)
	591 (3.63)	588 (3.84)	584 (3.63)	587 (3.59)	587 (3.61)	589 (3.53)

[a] Edge-to-edge distances. [b] Zn–C distance.

Absorption spectroscopy: The close proximity of the porphyrin and fullerene π-systems gives rise to through-space[23] and through-bond interactions, whose effects may be detectable in the shifts of some absorption bands or by the presence of new CT bands in the spectra of the four dyads. We show in the following that these features emerge here as sensitive markers for assessing the electronic coupling in **ZnP – C$_{60}$** ensembles. Red shifts of the Soret and Q-band transitions are consistently observed in the dyads and are reported in Table 1, in which similar data for the model porphyrin systems are also given. To a good extent, the shifts track the interchromophore separations (R_{ee}) of the donor – acceptor ensembles: **2** ($\lambda = 429$, 552, 591 nm; $R_{ee} = 3.0$ Å) > **4** ($\lambda = 427$,

551, 588 nm; $R_{ee} = 5.86$ Å) > **3**($\lambda = 425$, 549, 584 nm; $R_{ee} = 6.18$ Å). The reference values for the absorption of **ZnP** are 420 – 421, 548 – 549, and 587 – 589 nm. Deviations are observed for the highest Q-bands, which probably interact with other electronic states, and for **1**, which is characterized by bands only slightly shifted from the reference values, a feature indicative of small interfragment interactions. The data confirm the idea of the existence of a synergism between separation and overlap, as illustrated in Figure S1 in the Supporting Information.

At longer wavelengths ($\sim$700 nm) only the weak fullerene transitions ($\varepsilon \sim 200\,M^{-1}cm^{-1}$) should exist with maxima at 690 nm (mono-adduct), 696 nm (*trans*-2 bis-adduct) and 694 nm (equatorial bis-adduct).[24] However, subtraction of the fullerene absorption from the spectra of the four dyads reveals a new broad band in the 700 – 800 nm region. Since neither **ZnP** nor $\mathbf{C_{60}}$ exhibit this feature, it is safe to assign this additional band to a CT transition between the porphyrin donor and the electron-accepting fullerene. The presence of the additional band, therefore, confirms electronic interaction between the two chromophores in the dyads.

The intensity trend of the CT bands in toluene, reported in Table 2, is reminiscent of the trend observed for the spectral shifts described above. The most intense band ($\varepsilon_{max} = 1470$ M^{-1} cm^{-1}) appears for **2**, with its face-to-face structure, while only a weak band ($\varepsilon_{max} = 250$ M^{-1} cm^{-1}) is present for **3** with its face-to-edge orientation. As before, the data for **4** fall between the other two, while the intensity of the new band of **3** is the lowest. It should be further noted that the ordering of the interactions deduced by the band shifts and the relative intensities in the various dyads follows the anodic shifts of the reduction of the fullerene moiety.[18] For instance, in dyad **2** the first reduction is anodically shifted by nearly 100 mV, relative to that of **4**, while in **3** it is shifted to higher energies than for **2**.

Table 2. Charge transfer absorption and electronic coupling in different **ZnP** – $\mathbf{C_{60}}$ donor – acceptor ensembles in toluene at room temperature.

	2	**4**	**3**	**1**
R_{cc} [Å][a]	6.6	9.5	15.1	7.9
ε_{max} [$M^{-1}cm^{-1}$]	1470	740	250	10
$\tilde{\nu}_{max}$ [cm^{-1}]	13831	13717	14084	13550
$\tilde{\nu}_{1/2}$ [cm^{-1}]	961	847	900	$\sim$1000
V [cm^{-1}]	436	201	76	30

[a] Center-to-center distances as measured from the zinc center.

The CT spectra are used to estimate the electronic coupling element (V) by means of Equation (1):[25]

$$V = \frac{2.06 \times 10^{-2} (\varepsilon_{max} \nu_{max} \Delta\nu_{1/2})^{1/2}}{R_{cc}} \quad (1)$$

in which R_{cc} denotes the shortest center-to-center separation, ε_{max} the extinction coefficient, ν_{max} the energy, and $\nu_{1/2}$ the halfwidth of the CT transition. The electronic coupling in *trans*-2-**ZnP** – $\mathbf{C_{60}}$ (**2**), *meta*-**ZnP** – $\mathbf{C_{60}}$ (**4**), equatorial-**ZnP** – $\mathbf{C_{60}}$ (**3**), and *para*-**ZnP** – $\mathbf{C_{60}}$ (**1**) is 436, 201, 76, and 30 cm^{-1}, respectively.

The solvent effect on the CT band concurs with the ordering of the couplings obtained from Equation (1). Increasing the solvent polarity from toluene to benzonitrile leads to strong red shifts of the CT absorption in **2** and **4**—see Figure 3. The effect is caused by the better solvation that

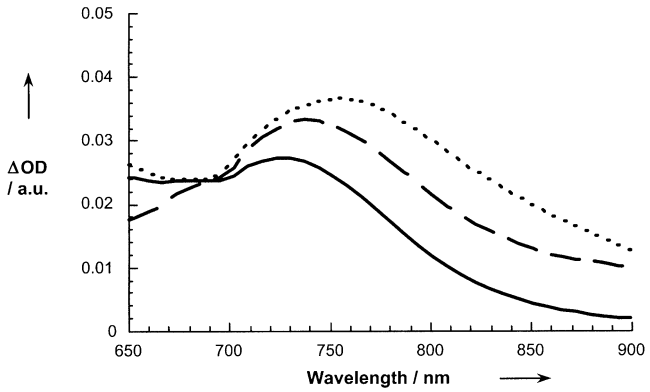

Figure 3. Charge-transfer absorption of dyad **2** in toluene (solid line), *o*-dichlorobenzene (dashed line) and benzonitrile (dotted line) at room temperature.

radical cations and/or radical anions experience in a more polar environment. As an example, Figure 3 illustrates the CT bands for **2** in toluene, *o*-dichlorobenzene, and benzonitrile, which shift from 723 nm to 732 nm and finally to 749 nm. In dyad **4** the maxima are also red-shifted upon increasing the solvent polarity: 727 nm in toluene, 730 nm in chloroform, 734 nm in *o*-dichlorobenzene, and 754 nm in benzonitrile. The weakness of the transition in **1** limited the validity of such an analysis.

The spectral analysis carried out on 1) the band shifts of the **ZnP** fragment, 2) the intensity of the newly formed CT bands, and 3) their shifts upon variation of the solvent polarity proves that the strength of electronic interaction between **ZnP** and $\mathbf{C_{60}}$ in the ground state is **2** > **4** > **3** > **1** and varies by more than an order of magnitude.

Fluorescence spectroscopy: To study the electronic interactions between the porphyrin and fullerene π-systems in the excited state, emission measurements were carried out with the **ZnP** – $\mathbf{C_{60}}$ dyads in solvents of different polarity (i.e., toluene, chloroform, THF, dichloromethane, *o*-dichlorobenzene, and benzonitrile). The ^{1}***ZnP** emission becomes quenched in all solvents for all **ZnP** – $\mathbf{C_{60}}$ dyads with quantum yields (Φ_F) usually of the order of 10^{-4} (Table 3)—in the **ZnP**

Table 3. Room temperature fluorescence quantum yields (^{1}***ZnP**) of different **ZnP** – $\mathbf{C_{60}}$ donor – acceptor ensembles in various solvents (excitation wavelength: 555 nm).

	2	**4**	**3**	**1**
toluene	1.26×10^{-4}	5.50×10^{-4}		15.9×10^{-4}
chloroform	1.31×10^{-4}	3.58×10^{-4}	6.8×10^{-4}	15.8×10^{-4}
THF	1.16×10^{-4}	3.68×10^{-4}	12.0×10^{-4}	15.6×10^{-4}
dichloromethane	1.37×10^{-4}	1.81×10^{-4}	4.4×10^{-4}	14.9×10^{-4}
o-dichlorobenzene	1.43×10^{-4}		9.5×10^{-4}	
benzonitrile	1.37×10^{-4}	3.42×10^{-4}	5.6×10^{-4}	12.6×10^{-4}
DMF		2.91×10^{-4}	4.3×10^{-4}	12.1×10^{-4}

reference $\Phi_F = 0.04$. Although the yield drops, the **ZnP** emission patterns are not affected by the presence of the fullerene fragment.

A close inspection of the fluorescence data reveals a number of interesting features:

1) The fluorescence quantum yield of dyad **2** does not change appreciably with the solvent. This is attributed to the intramolecular charge-transfer reaction, which is mediated through the overlapping π-orbitals and does not use bridging solvent molecules.
2) The two dyads with the largest edge-to-edge separation (R_{ee}), that is **4** (5.86 Å) and **3** (6.18 Å), show a similar solvent dependence, that is, appreciably stronger fluorescence quenching in the polar solvents than in the nonpolar media.
3) Dyad **1** has a small interchromophore distance (3.23 Å) but a poor spatial overlap and reveals the strongest ^{1}***ZnP** fluorescence.

Interestingly, the greater the fluorescence quenching, the larger is the electronic coupling that was determined from the ground-state absorption spectra. This indicates that if major rearrangements occur in the excited state, they are already present in the spectra.

Not all dyads emit uniquely from **ZnP**: emission was also observed from $\mathbf{C_{60}}$ in **3** at ~765 nm with $\Phi_F = 2.2 \times 10^{-4}$ in toluene, that is, about half of that measured for the $\mathbf{C_{60}}$ reference,[24] while in chloroform, the same fullerene emission was seen with a lower quantum yield (1.1×10^{-4}). Further increase of the solvent polarity, for example, use of THF led to a complete cancellation of the $\mathbf{C_{60}}$ emission through enhancement of the ET process. Emission from $\mathbf{C_{60}}$ after excitation of **ZnP** implies energy transfer, which was confirmed by a set of excitation spectra.[26] For a Coulombic energy transfer, the distance dependence (R_{ee}) is defined by Equation (2):

$$k = k_D \left(\frac{R_C}{R_{ee}}\right)^6 \quad (2)$$

in which $k_D = 4.0 \times 10^8\ s^{-1}$ is the intrinsic deactivation of the photoexcited ^{1}***ZnP**, and R_C is the critical transfer radius at which k equalizes the intrinsic deactivation of the donor.[27] Considering R_{ee} and R_C equal 6.18 and 9.78 Å, respectively, a rapid energy transfer with $k = 7.2 \times 10^9\ s^{-1}$ is estimated; this is in good agreement with the experimental value ($\sim 10^{10}\ s^{-1}$).

In the two closer packed dyads, namely, **1** and **2**, the $\mathbf{C_{60}}$ fluorescence is not observed even in toluene. This implies that the shorter donor–acceptor separation alters the deactivation mechanism of ^{1}***ZnP**, that is, ET takes over with respect to energy transfer. Forasmuch as the small reorganization energy of, for example, **2** in toluene (vide infra), which also infers negligible activation barriers for ET, the distance dependence can be formulated in a first approximation within the framework of the Dexter double electron exchange mechanism [Eq. (3)]:

$$k = \frac{4\pi(V_0 \exp[-0.5(R_{ee} - R_0)])^2}{\hbar} J \quad (3)$$

in which V is the electronic coupling element and J is the pertinent spectral overlap of orbitals involved in ET reactions ($5.04 \times 10^{-4}\ cm^{-1}$).[28] This leads to rate constants $\geq 10^{12}\ s^{-1}$.

The emission spectra therefore indicate that at short donor–acceptor separations ($R_{ee} \sim 3$ Å) ET takes place even in toluene and that a larger distances transfer of singlet excited state energy may occur when the solvent polarity is sufficiently low. In more polar media the picture is somewhat different; ET dominates, regardless of the separation.

Charge transfer emission: Apart from the **ZnP** and the occasional $\mathbf{C_{60}}$ fluorescence, the dyads show rather broad emission in the region located around 800 nm—see Figure 4.[29] The new band is assigned to CT emission in analogy

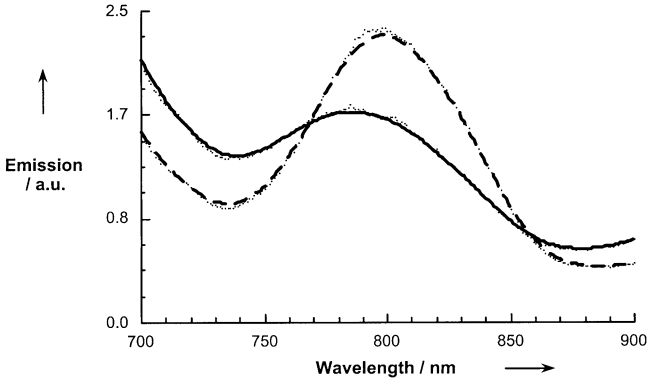

Figure 4. Charge transfer emission of $\mathbf{ZnP-C_{60}}$ (**4**: solid line) and (**2**: dashed line) in toluene at 77 K ($\sim 1.0 \times 10^{-5}$ M); excitation wavelength 560 nm.

with the CT absorption bands discussed earlier (vide supra). Similar interpretations were reported previously for two different $\mathbf{ZnP-C_{60}}$ systems.[25, 30] At low temperature (77 K) the emission bands, which are rather broad at room temperature, are resolved, in accordance with the assumption that its width is determined by $(4\lambda_S k_B T)^{1/2}$. Illustrative examples are shown in Figure 4, with the maximum at 800 nm for **2** and 785 nm for **4**. The former is characterized by a π-stacked system and has a CT absorption at slightly higher energies. The energy difference between absorption and emission, or Stokes shift, is quite small (0.17 eV for **2** and 0.12 eV for **4**). In turn, this gives vibrational reorganization energies (λ_V) of 0.09 ± 0.02 and 0.06 ± 0.01 eV. Support for these remarkably small λ_V values also derives from an earlier theoretical calculation of the vibrational reorganization energy of $\mathbf{C_{60}}$ ($\lambda_V = 0.06$ eV).[31] The π-stacked dyad reveals a notably larger value, which is indicative of the perturbation due to the overlapping π-systems. This conclusion is in agreement with the relatively strong coupling estimated for this donor–acceptor ensemble (vide supra).

The position of the CT emission band (1.58 eV and 1.54 eV) can be further used to determine the solvent reorganization energy (λ_S), since the excitation energy is given by $-(\lambda_S + \Delta G_{CR}^{\circ})$. Thus, λ_S values of 0.1 ± 0.01 eV and 0.02 ± 0.01 eV result for **4** and **2**, respectively. The different values of λ_S suggests that solvation is, therefore, more efficient in the former than in the latter, inducing stronger solvent interactions with the **ZnP** and $\mathbf{C_{60}}$ moieties. As noted earlier, in dyad **2**, most of the porphyrin surface is covered by the fullerene.

Charge-separation dynamics: The fate of ^{1}***ZnP** and the identity of the photoproducts in the dyads were examined by pico-/nano-/microsecond transient absorption spectroscopies.

Representative picosecond time-resolved absorption spectra, taken after an 18 ps laser pulse at 532 nm[32] for a solution of **ZnP** in toluene as a reference, are displayed in Figure 5a.

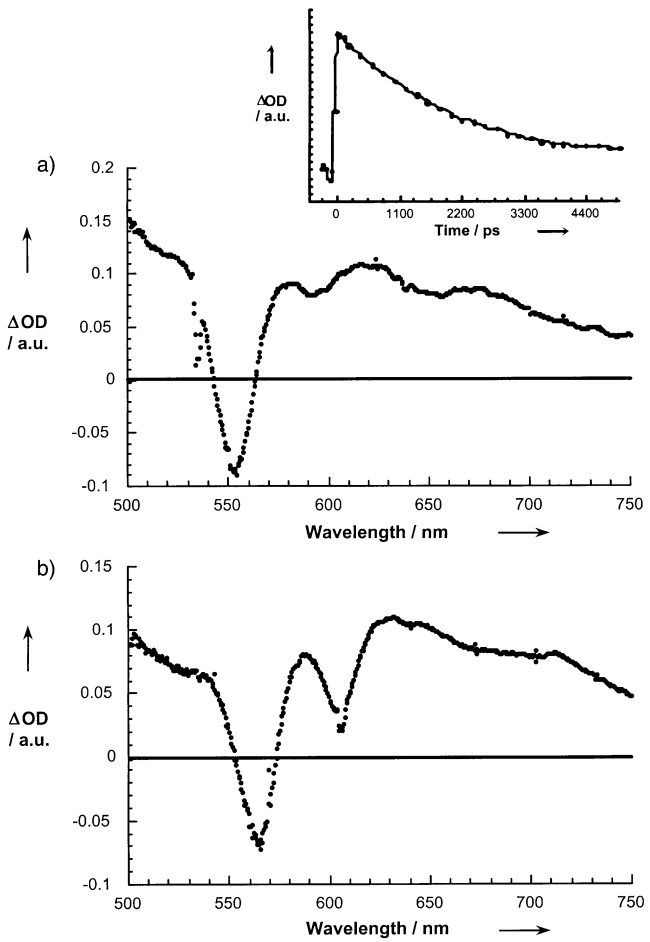

Figure 5. Picosecond transient absorption spectrum recorded 50 ps upon flash photolysis of **ZnP** (5.0×10^{-5} M) at 532 nm in deoxygenated a) toluene and b) benzonitrile, indicating the **ZnP** singlet – singlet absorption. The insert to a) illustrates the intersystem crossing process in photoexcited **ZnP**.

The differential spectrum recorded immediately after the laser pulse (50 ps time delay) is characterized by bleaching of the porphyrin Q-band absorption at 550 nm and broad absorption between 570 and 750 nm. These spectral attributes are indicative of the **ZnP** singlet excited state ($E_{\text{Singlet}} =$ 2.00 eV), which decays slowly (4.0×10^8 s^{-1}) to the energetically lower-lying triplet excited state ($E_{\text{Triplet}} = 1.53$ eV) predominantly through intersystem crossing (**ZnP** triplet quantum yield, Φ_{Triplet}: 0.88). The formation of a penta-coordinate Zn environment in coordinating solvents, such as THF, benzonitrile (Figure 5b)[13] and DMF, shifts the Q-band slightly to the red, to 565 nm, with respect to the non-coordinating solvents toluene and dichloromethane.

Next, the transient absorption changes of **ZnP** – $\mathbf{C_{60}}$ donor – acceptor ensembles were recorded in toluene with several time delays after the 532 nm picosecond laser pulse and compared with what was seen for the **ZnP** reference. At early times (i.e., 50 – -100 ps), these are practically identical to those of the **ZnP** reference, disclosing strong bleaching at 550 nm (similar to Figure 5a/b). However, at a delay time of 200 ps, a new transition around 640 nm grows-in (Figure 6a) accompanied by another absorption in the near-infrared. Based on a spectral comparison, we ascribe the former to the zinc porphyrin π-radical cation (**ZnP**$^{\bullet+}$), while the latter band belongs to the fullerene π-radical anion ($\mathbf{C_{60}}^{\bullet-}$).[24] In accordance with these results, we propose that CS, from the **ZnP** singlet excited state to the electron-accepting fullerene, creates the **ZnP**$^{\bullet+}$ – $\mathbf{C_{60}}^{\bullet-}$ state, which is responsible for the

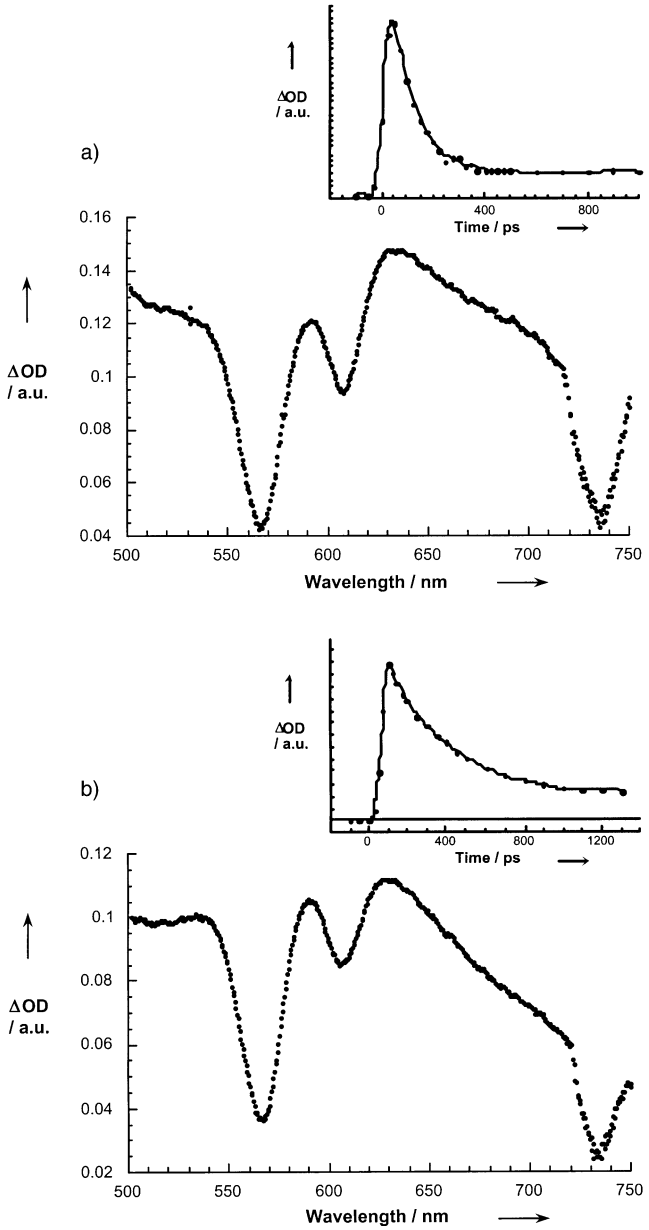

Figure 6. Picosecond transient absorption spectrum recorded a) 400 ps and b) 50 ps upon flash photolysis of **4** and **2** (5.0×10^{-5} M), respectively at 532 nm in deoxygenated toluene, indicating the **ZnP** π-radical cation absorption. Inserts show the decay of *meta*-^{1}***ZnP** – $\mathbf{C_{60}}$ (@610 nm) and *trans*-2-**ZnP**$^{\bullet+}$ – $\mathbf{C_{60}}^{\bullet-}$ (@630 nm).

fast deactivation of the photoexcited chromophore. The absorption of the charge-separated $\mathbf{ZnP}^{\bullet+}-\mathbf{C_{60}}^{\bullet-}$ pair is persistent on the picosecond timescale and decays in the nano-/microseconds regime (vide infra).

Similar spectral characteristics of $\mathbf{ZnP}^{\bullet+}$ and $\mathbf{C_{60}}^{\bullet-}$ were found for all the donor–acceptor ensembles in THF, dichloromethane, benzonitrile, and DMF.[33] Table 4 indicates that the lifetimes of the ^{1}***ZnP** substantially decreased with the solvent polarity and ranged from 149 to 28 ps. It should be noted that the different functionalization pattern of the fullerene core leads to different λ_{max} values for the corresponding C_{60} π-radical anion fingerprints: 900 nm (**2**), 1000 nm (**1**) and 1060 nm (**3**) (Figure 7). The values are in excellent agreement with those found in an independent pulse radiolysis study, which focused on the free radical-induced reduction of a series of methanofullerene derivatives.[24]

Table 4. Singlet excited state lifetimes of ^{1}***ZnP** [in ps] in different **ZnP**–$\mathbf{C_{60}}$ donor–acceptor ensembles in various solvents (excitation wavelength: 532 nm).

	4	**3**	**1**
toluene	52	[a]	132
chloroform	36	[a]	115
THF	35	149	130
dichloromethane	28	47	107
benzonitrile	[b]	55	103
DMF	[b]	35	97

[a] Energy transfer. [b] Not measured.

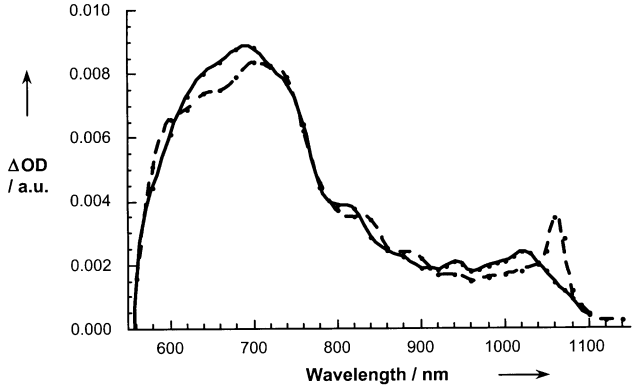

Figure 7. Nanosecond transient absorption spectrum (visible/near-infrared part) recorded 50 ns upon flash photolysis of **3** (5.0×10^{-5} M, dashed line) and **4** (5.0×10^{-5} M, solid line) at 532 nm in deoxygenated benzonitrile, indicating the **ZnP** π-radical cation and $\mathbf{C_{60}}$ π-radical anion absorption.

A final comment should address the photophysical properties of **2**. The rate of intramolecular CS is essentially within the time-resolution of our apparatus ($\geq$20 ps). Instead, the differential absorption changes, typically noted immediately after the 20 ps laser pulse, are already composed of the individual contributions stemming from the oxidized donor (Figure 6b) and reduced acceptor.

Charge recombination dynamics: The charge recombination (CR) dynamics were analyzed by following the absorption changes of the one-electron reduced form of the electron acceptor ($\mathbf{C_{60}}^{\bullet-}$) and that of the one-electron oxidized form of the electron donor ($\mathbf{ZnP}^{\bullet+}$) (as an example, see Figure 7).

In oxygen-free solutions, the decays were well fitted by a single exponential expression. Charge separation (CS) and charge recombination (CR) rates, quantum yields, and thermodynamic parameters are shown in Tables 5 and Table 6; see also the Supporting Information (Section S3) for details on their estimation. As far as the thermodynamics are concerned, the larger the solvent polarity the less negative is the free energy associated with CR, while the opposite trend holds for CS.

Table 6. Lifetimes (τ) and quantum yields (Φ) of the $\mathbf{ZnP}^{\bullet+}-\mathbf{C_{60}}^{\bullet-}$ radical pair formed in different **ZnP**–$\mathbf{C_{60}}$ donor-acceptor ensembles (excitation wavelength: 532 nm).

	2	**4**		**3**		**1**	
	τ [ps]	τ [ns]	Φ	τ [μs]	Φ	τ [ns]	Φ
toluene ($\varepsilon=2.38$)	619	395	0.19	[a]	–	–	0.28
THF ($\varepsilon=7.6$)	385	215	0.45[b]	2.6	0.28	236	0.47[b]
dichloromethane ($\varepsilon=9.08$)	121	195	0.44	1.85[c]	0.36	207	0.42
benzonitrile ($\varepsilon=24.8$)	38	113	0.27	1.1	0.20	149	0.36
DMF ($\varepsilon=36.7$)	[d]	99	0.17	0.21	0.06	133	0.25

[a] Energy transfer. [b] In chloroform. [c] In *o*-dichlorobenzene ($\varepsilon=9.98$). [d] Not measured.

Inspection of Table 6 reveals that the differences in electronic coupling affect the lifetimes of the $\mathbf{ZnP}^{\bullet+}-\mathbf{C_{60}}^{\bullet-}$ radical pair, with actual values ranging from the picosecond and nanosecond to the microsecond regime. Regardless of the solvent, the ordering of the lifetimes is: $\mathbf{2}<\mathbf{4}<\mathbf{1}<\mathbf{3}$. For all dyads, the higher the solvent polarity, the shorter the lifetime of the charge-separated state. A decrease of $-\Delta G^{\circ}$ and faster CR kinetics is typical of Marcus inverted region, whereby the ET rates start to decrease with increasing free-energy change.[34] From the best fits of the driving force dependence on CR rates [Eq. (4)]:

$$k_{ET}=\left(\frac{4\pi 3}{h^2\lambda k_B T}\right)^{1/2}V^2\exp\left(\frac{-\Delta G^{o}}{k_B T}\right) \quad (4)$$

Table 5. Thermodynamic parameters ($-\Delta G^{o}_{CS}$, $-\Delta G^{o}_{CR}$) for different **ZnP**–$\mathbf{C_{60}}$ donor-acceptor ensembles.

	2		**4**		**3**		**1**	
	$-\Delta G^{o}_{CS}$ [eV]	$-\Delta G^{o}_{CR}$ [eV]	$-\Delta G^{o}_{CS}$ [eV]	$-\Delta G^{o}_{CR}$ [eV]	$-\Delta G^{o}_{CS}$ [eV]	$-\Delta G^{o}_{CR}$ [eV]	$-\Delta G^{o}_{CS}$ [eV]	$-\Delta G^{o}_{CR}$ [eV]
toluene ($\varepsilon=2.38$)	0.44	1.56	0.32	1.68			0.46	1.54
THF ($\varepsilon=7.6$)	0.54	1.46	0.78	1.22	0.61	1.39	0.56	1.44
dichloromethane ($\varepsilon=9.08$)	0.55	1.45	0.82	1.18	0.67	1.33	0.57	1.43
benzonitrile ($\varepsilon=24.8$)	0.57	1.43	0.94	1.06	0.79	1.21	0.59	1.41
DMF ($\varepsilon=36.7$)			0.96	1.04	0.82	1.18	0.60	1.40

the following values for the reorganization energies (λ) and the electronic couplings (V) were derived: $\lambda = 0.71$ eV and $V = 313\ cm^{-1}$ for **2**; $\lambda = 0.54$ eV and $V = 10\ cm^{-1}$ for **3**.[35] Interestingly, the trend seen for V derived from the fit of ET rates further substantiates the values calculated based on the CT absorption, although the absolute magnitude is slightly different.

Finally, the close π-stacking in **2** seems to lead to a significant perturbation of the overlapping π-systems. This is, for example, expressed by the somewhat larger reorganization energy (λ) found for **2** relative to **3** and **4**. Note that the energetic difference between the CT absorption and CT emission (vide supra), as an independent measure for λ, led to the same conclusion.

Dynamical modeling of the electronic coupling: Molecular dynamics trajectories for the two limiting cases of **2** and **3** were calculated in the gas phase and in three different solvents (i.e., toluene, dichloromethane, and benzonitrile). The solvent was treated explicitly to allow for the possibility of a molecule inserting between the acceptor and the donor.[36] The calculations were run with the TINKER package[37] with the MM3 force field,[38] which has found a wide range of applications in one of our laboratories.[39] The force field was corrected to account for the charge distribution on the **ZnP**$^{\bullet+}$ – **C**$_{60}^{\bullet-}$ species by adding point charges, which were calculated as the difference between the Mulliken charges of the CT state and the ground state (see also below). The simulation box, with periodic boundary conditions, gave a minimum distance between solute molecules of 16 Å; the cutoff for the van der Waals interactions was set to 8 Å. All solvents were added using room temperature densities. The solvents were considered explicitly to include the effect of specific solvation. The molecular dynamnics (MD) calculations were run at a constant temperature of 300 K, within the canonical ensemble, using the Berendsen algorithm.[40] Hydrogen atoms were constrained to their ideal bond length by using the RATTLE algorithm[41] and the time step was 1 fs. After an initial equilibration of 30 ps, snapshots for the evaluation of the electronic coupling matrix element were taken every 0.1 ps. The coupling V was calculated, with the INDO/S plus configuration interaction singles model,[42] for the CR process. The CT state is mainly described as the one-electron excitation from the HOMO of **ZnP** and the LUMO of **C**$_{60}$. In this simple picture, the coupling between the ground state and the CT state can be formulated as Equation (5):[43]

$$V = \langle \phi^0_{\mathrm{HOMO(ZnP)}} \mid F^0 \mid \phi^0_{\mathrm{LUMO(C60)}} \rangle \qquad (5)$$

in which F is the Fock operator and the suffix zero indicates that the orbitals are unperturbed and localized either on **ZnP** or on **C**$_{60}$. The approach does not include through-bond coupling, which is less important and roughly similar for the two dyads. Illustrative plots of the coupling V versus time are given in Figure 8, whereby V undergoes large fluctuations on the timescale of CT reactions. In hindsight, the fluctuations seen in Figure 8 further assert the need to carry out dynamic simulation. Importantly, the MD was run until the time average value of V achieved convergence. Table 7 gives the values of V together with the calculated standard deviation calculated for the dynamics of the dyad in the ground and with the charges of its CT state.

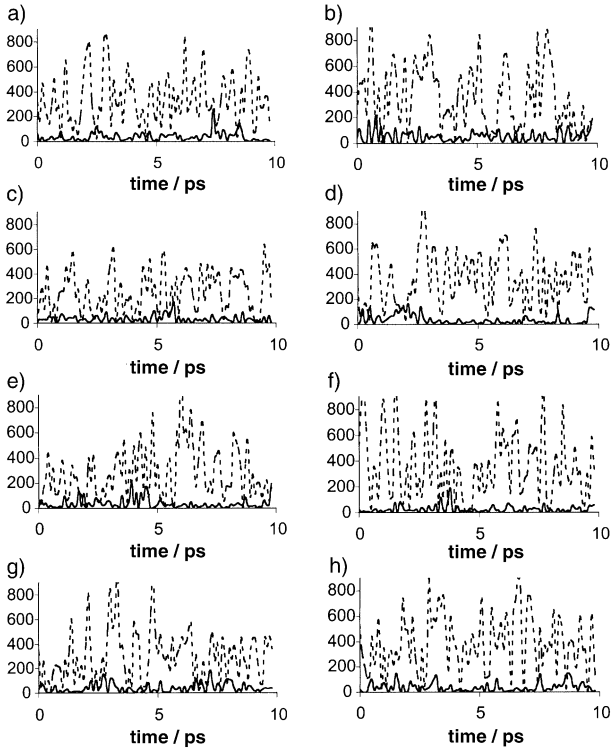

Figure 8. Molecular dynamics simulation of the electronic coupling matrix element: a) gas phase, ground state; b) gas phase, CT state; c) in toluene, ground state; d) in toluene, CT state; e) in CH_2Cl_2, ground state; f) in CH_2Cl_2, CT state; g) in benzonitrile, ground state; h) in benzonitrile, CT state; solid line **3**, dashed line **2**.

Table 7. Calculated electronic coupling (V) in cm^{-1}.

	2		**3**	
	ground state	CT state	ground state	CT state
gas phase	339 ± 20	358 ± 24	37.6 ± 3.6	54.5 ± 4.4
toluene	257 ± 17	364 ± 21	34.5 ± 2.8	36.7 ± 3.8
dichloromethane	280 ± 21	360 ± 26	36.0 ± 4.0	25.7 ± 2.8
benzonitrile	314 ± 22	387 ± 22	41.2 ± 3.7	37.3 ± 3.5

The couplings depend weakly on the solvent, a finding that justifies this assumption in the fitting procedure of the experimental data. For **2**, they range from 257 cm^{-1} in the ground state in toluene to 387 cm^{-1} in the CT state in benzonitrile, while for **3** they vary from 34 cm^{-1} in the ground state in toluene to 54 cm^{-1} for the CT state in the gas phase. These values can be compared with 436 cm^{-1} obtained from the spectral analysis of **2** for which the fitting of the CR data gave 313 cm^{-1}. Also a value of 76 cm^{-1} was obtained from the spectral analysis of **3**, while the fitting of the CR data gave 10 cm^{-1}.

The calculations therefore confirm the order of magnitude of difference for V in the two dyads. The larger couplings found in the molecular dynamics simulations that used the charges of the CT state are due to the presence of increased Coulomb forces, which bring the two moieties closer. Ideally,

the coupling in the Marcus treatment should be calculated at the crossing of the potential-energy surfaces. In the present case, an average of the values for the two states should be a rather good approximation to such a value.

The reorganization energy (λ) was also estimated with an "instantaneous" approach. At each of the snapshots of the dynamics the partial atomic charges were switched from those of one state to those of the other and the energy was recalculated—see Figure 9. In the dynamics of the ground

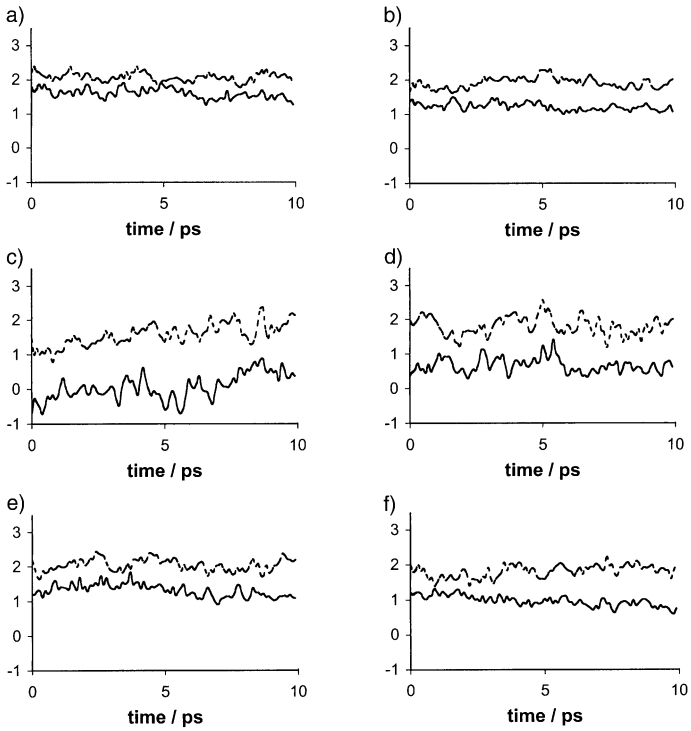

Figure 9. Molecular dynamics simulation of the reorganization energy (λ): a) in toluene, ground state; b) in toluene, CT state; c) in CH_2Cl_2, ground state; d) in CH_2Cl_2, CT state; e) in benzonitrile, ground state; f) in benzonitrile, CT state; solid line **3**, dashed line **2**.

state, the sudden appearance of the charges of the CT state increases the energy (the same happens in the dynamics of the CT state when the atomic charges used are those of the ground state). Time averaging the energy differences over the dynamics gives the results, listed in Table 8.

Table 8. Estimated reorganization energy (λ) in eV.

	2	**3**
toluene	0.26 ± 0.01	0.34 ± 0.01
dichloromethane	0.77 ± 0.02	0.61 ± 0.02
benzonitrile	0.43 ± 0.01	0.38 ± 0.01

Several points are worth noticing:

1) λ is solvent dependent, but does not vary too markedly. This justifies the assumptions in the fitting of the experimental data, at least as a first approximation.
2) For **2**, λ ranges from 0.26 to 0.77 eV, while for **3** λ varies from 0.34 to 0.61 eV. These values can be compared with a) $\lambda_V + \lambda_S = 0.09 + 0.02 = 0.11$ eV obtained from the spectral analysis of **2**, while the fitting of the CR data in several solvents gave 0.74 eV and b) 0.54 eV obtained from the fitting of the CR data of **3**. The disagreement between the two analysis of the experimental data is solved in favor of the results of the fitting of the CR kinetics by the molecular dynamics calculations.
3) Dichloromethane has the largest λ value (0.77 eV for **2** and 0.61 eV for **3**). This is in keeping with the notion that the phenyl rings of toluene and benzonitrile match the shapes of $\mathbf{C_{60}}$ and **ZnP** by forming π-stack complexes. Atomic charge variations affect such stacks only mildly. On the contrary, the shape of dichloromethane does not fit with that of the two charged moieties, and even small charge variation may cause a large rotational reorganization of this solvent.
4) The effect of the large reorganization energy in dichloromethane finds experimental confirmation. Table 5 shows that the free energy for CS of **3** in this solvent from the excited state to the charge-separated state is 0.67 eV, which is very similar to the calculated reorganization energy, 0.61 eV. In turn, this implies that the potential-energy curve of the CT state crosses the excited state near its minimum. The resulting effect is very fast conversion of the excited state to the CT state. Table 6 shows that upon excitation the yields of the charge-separated state of **3** in dichloromethane is the largest of the three solvents studied.
5) The similarity of the reorganization energy for **2** and **3** makes the large difference in electronic coupling even more relevant to the issue of this work, and supports the proposal that **ZnP**–$\mathbf{C_{60}}$ systems are excellent choices to study the effect of topological variations on ET rates.

Conclusion

In conclusion, the photo-induced ET in four different **ZnP**–$\mathbf{C_{60}}$ dyads has been studied. The distance and orientation between electron acceptor and electron donor varies substantially, in a consistent way, as a function of the mechanical link. This feature makes them a good case for verifying the generally accepted rules on the distance dependence of ET. For the first time, spectral analysis was carried out comprehensively on 1) the band shifts of the **ZnP** fragment, 2) the intensity of newly formed CT bands, and 3) their spectral shifts upon variation of the solvent polarity. All the results agree quantitatively and show that the strength of interaction between **ZnP** and $\mathbf{C_{60}}$ varies more than an order of magnitude and scales with the **ZnP**–$\mathbf{C_{60}}$ distance (i.e., *trans*-2-**ZnP**–$\mathbf{C_{60}}$ (**2**) > *meta*-**ZnP**–$\mathbf{C_{60}}$ (**4**) > equatorial-**ZnP**–$\mathbf{C_{60}}$ (**3**) > *para*-**ZnP**–$\mathbf{C_{60}}$ (**1**)). Also the quantum yields of formation of ^{1}***ZnP** were found to be a function of the same distance.

The different strength in electronic coupling affects sensitively both CS and CR kinetics—no change in mechanism occurs. Most importantly, the lifetime of the $\mathbf{ZnP^{\bullet+}}$–$\mathbf{C_{60}^{\bullet-}}$ radical pair, product of an intramolecular CS event evolving from ^{1}***ZnP** (i.e., 532 nm excitation) or ^{1}***$\mathbf{C_{60}}$** (i.e., 355 nm excitation), exhibits values that range from the picosecond and nanosecond to the microsecond regime.

Apart from the spectral analysis, the interactions between **ZnP** and $\mathbf{C_{60}}$ were quantitatively evaluated in two other ways: by fitting the CR rates and by molecular dynamics calculations. The three approaches gave a rather consistent picture. For instance, molecular dynamics calculations for **2** gave $257 = V = 387\ cm^{-1}$ as compared with $313 = V = 436\ cm^{-1}$ obtained by fitting of the experimental data, while for **3** they gave $34 = V = 54\ cm^{-1}$ as compared with $10 = V = 76\ cm^{-1}$ obtained by fitting of the experimental data. Similar calculations gave for **2** $0.26 = \lambda = 0.77$ eV as compared with $0.11 = \lambda = 0.74$ eV obtained by fitting of the experimental data, while for **3** they gave $0.34 = \lambda = 0.61$ eV as compared with 0.54 eV from fitting of experimental data.

Experimental Section

General: Picosecond laser-flash photolysis experiments were carried out with 532 nm laser pulses from a mode-locked, Q-switched Quantel YG-501 DP Nd:YAG laser system (18 ps pulse width, 2 – 3 mJ per pulse). Nanosecond laser-flash photolysis experiments were performed with laser pulses from a Quanta-Ray CDR Nd:YAG system (532 nm, 6 ns pulse width) in a front face excitation geometry.

Fluorescence lifetimes were measured with a laser strope fluorescence lifetime spectrometer (Photon Technology International) with 337 nm laser pulses from a nitrogen laser fiber coupled to a lens-based T-formal sample compartment equipped with a stroboscopic detector. Details of the Laser Strobe systems are described on the manufacture's web site (http://www.pti-nj.com).

Emission spectra were recorded with a SLM 8100 spectrofluorometer. The experiments were performed at room temperature. Each spectrum represents an average of at least 5 individual scans, and appropriate corrections were applied whenever necessary.

Synthesis of 3-[2-(methoxymalonyloxy)ethoxy]benzaldehyde (6): A solution of 3-[2-hydroxyethoxy]benzaldehyde (12.0 g, 0.072 mol) and pyridine (6.5 mL, 0.081 mol) in dichloromethane (100 mL) was cooled down to 0 °C. Subsequently methyl malonyl chloride (8.0 mL, 0.084 mol) was added and the reaction mixture was stirred for 1 hour at 0 °C and another hour at RT. The precipitate was dissolved in water and the organic phase was extracted twice with 0.1N HCl, once with $NaHCO_3$ and dried over $MgSO_4$. After evaporation of the solvent a yellow oil was obtained. Yield: 15.98 g (0.060 mol), 83 % referred to 3-[2-hydroxyethoxy]benzaldehyde. FT-IR (film): $\tilde{\nu} = 3068, 3004, 2956, 2845, 1738, 1447, 1386, 1262, 790, 684\ cm^{-1}$; MS (EI): *m/z* (%): 266 (10) $[M]^+$, 166 (35), 145 (90), 121 (100).

Synthesis of 5-{3-[2-(methoxymalonyloxy)ethoxy]phenyl}-10,15,20-triphenylporphyrin 7: A solution of **6** (6.65 g, 25.0 mmol), benzaldehyde (2.53 mL, 25.0 mmol), pyrrole (3.50 mL, 50.0 mmol) and Ph_4PCl (58 mg, 0.15 mmol) in dichloromethane (500 mL) was stirred for 10 min under a nitrogen atmosphere before $BF_3 \cdot Et_2O$ (628 μL, 5.0 mmol) were added. After one hour *para*-chloranil (9.25 g, 37.6 mmol) was added under light protection and the reaction mixture was refluxed for another hour. The solvent was evaporated and the mono-functionalized porphyrin was separated by flash chromatography as the second fraction (SiO_2, CH_2Cl_2/EtOAc 20:1). Yield: 527 mg (0.68 mmol), 5.4 % referred to pyrrole. ^{1}H NMR (400 MHz, $CDCl_3$): $\delta = 8.84$ (m, 8H; β-C*H*), 8.21 (AA′BB′, 6H; Ar*H*), 7.85 ppm (d, 1H; Ar*H*); ^{1}H NMR (400 MHz, $CDCl_3$): $\delta = 9.98$ (s, 1H; C*H*O), 7.48 (m, 2H; Ar*H*), 7.40 (s, 1H; Ar*H*), 7.21 (m, 1H; Ar*H*), 4.54 (t, $^3J = 4.64$ Hz, 2H; CH_2), 4.26 (t, $^3J = 4.76$ Hz, 2H; CH_2), 3.73 (s, 3H; OCH_3), 3.45 ppm (s, 2H; CO–CH_2–CO); ^{13}C NMR (100.5 MHz, $CDCl_3$): $\delta = 191.84$ (*C*HO), 166.65, 166.34 (*C*=O), 158.90, 137.78 (C_{aromat}), 130.15, 123.94, 121.89, 112.77 (*C*H$_{aromat}$), 65.82, 63.44 (*C*H$_2$), 52.48 (O*C*H$_3$), 41.05 (1H; Ar*H*), [7.78 (s, 1H; Ar*H*), 7.75 (m, 9H; Ar*H*), 7.63 (t, 1H; Ar*H*), 7.30 (d, 1H; Ar*H*), 4.57 (t, $^3J = 4.64$ Hz, 2H; CH_2), 4.36 (t, $^3J = 4.64$ Hz, 2H; CH_2), 3.68 (s, 3H; OCH_3), 3.44 (s, 2H; CO–CH_2–CO), −2.57 ppm (br s, 2H; N*H*)]; ^{13}C NMR (100.5 MHz, $CDCl_3$): $\delta = 166.76$, 166.50 (*C*=O), 156.77, 143.63, 143.06, 142.13 (C_{aromat}), 134.55 (*C*H$_{aromat}$), 131.15 (β-*C*H), 128.17, 127.72, 127.61, 126.68, 121.12 (*C*H$_{aromat}$), 120.28, 119.48, 118.73 (*meso-C*), 114.20 (*C*H$_{aromat}$), 65.86, 63.85 (*C*H$_2$), 52.54 (O*C*H$_3$), 41.17 ppm (CO–*C*H$_2$–CO); UV/Vis (CH_2Cl_2): λ_{max} ($\log\varepsilon$) = 399 (sh, 4.87), 418 (5.65), 514 (4.21), 549 (3.77), 591 (3.63), 645 nm (3.42); FT-IR (KBr): $\tilde{\nu} = 3316, 3054, 3024, 2950, 1736, 1596, 1575, 1471, 1440, 1349, 1178, 1152, 964, 801, 730, 700\ cm^{-1}$; MS (MALDI-TOF): *m/z*: 775 $[M+H]^+$.

Synthesis of 5-{3-[2-(methoxymalonyloxy)ethoxy]phenyl}-10,15,20-triphenylporphyrinatozinc(II) (5): A solution of **7** (250 mg, 0.32 mmol) and $Zn(OAc)_2 \cdot 2H_2O$ (50 mg, 0.37 mmol)in THF (50 mL) was refluxed for one hour. The product was separated by flash chromatography (SiO_2, CH_2Cl_2/EtOAc 20:1). Yield: 260 mg (0.31 mmol), 97 % referred to **7**. ^{1}H NMR (400 MHz, $CDCl_3$): $\delta = 8.94$ (m, 8H; β-C*H*), 8.21 (AA′BB′, 6H; Ar*H*),7.85(d, 1H; Ar*H*), 7.74 (m, 10H; Ar*H*), 7.63 (t, 1H; Ar*H*), 7.28 (d, 1H; Ar*H*), 4.51 (t, $^3J = 4.64$ Hz, 2H; CH_2), 4.32 (t, $^3J = 4.76$ Hz, 2H; CH_2), 3.65 (s, 3H; OCH_3), 3.36 (s, 2H; CO–CH_2–CO); ^{13}C NMR (100.5 MHz, $CDCl_3$): $\delta = 166.71$, 166.45 (*C*=O), 156.66 (C_{aromat}), 150.26, 150.03 (α-*C*), 144.31, 142.81 (C_{aromat}), 134.42 (*C*H$_{aromat}$), 132.03, 131.99, 131.86 (β-*C*H), 128.50, 127.46, 126.55 (*C*H$_{aromat}$), 121.18 (*meso-C*), 120.98 (*C*H$_{aromat}$), 120.48 (*meso-C*), 114.11 (*C*H$_{aromat}$), 65.86, 63.83 (*C*H$_2$), 52.50 (O*C*H$_3$), 41.08 (CO–*C*H$_2$–CO); UV/Vis (CH_2Cl_2): λ_{max} ($\log\varepsilon$) = 399 (sh, 4.54), 417 (5.68), 548 (4.24), 587 nm (3.47); MS (FAB): *m/z*: 838 $[M+H]^+$.

Synthesis of dyad 4: A solution of the porphyrin malonate **5** (200 mg, 0.24 mmol) was stirred together with C_{60} (186 mg, 0.26 equiv) at RT for 24 h in toluene (150 mL) in the presence of 1,8-diazabicyclo[5,4,0]undec-7-en (DBU; 100 μL, 0.67 mmol) and I_2 (61 mg, 0.24 mmol). Chromatographic separation was performed on silica gel with toluene/ethylacetat (20:1) as eluent. Yield 134 mg, 36 % referred to **5**. ^{1}H NMR (400 MHz, $CDCl_3$): $\delta =$ 8.81 (m, 4H; β-C*H*), 8.77 (m, 4H; β-C*H*), 8.19 (AA′BB′, 1H; Ar*H*), 8.12 (AA′BB′, 1H; Ar*H*), 8.08 (AA′BB′, 1H; Ar*H*), 8.01 (AA′BB′, 2H; Ar*H*), 7.80 (d, 1H; Ar*H*), 7.68 (m, 10H; Ar*H*), 7.40 (m, 1H; Ar*H*), 7.25 (d, 1H; Ar*H*), 4.78 (t, $^3J = 4.76$ Hz, 2H; CH_2), 4.41 (t, $^3J = 4.76$ Hz, 2H; CH_2), 3.93 ppm (s, 3H; OCH_3); ^{13}C NMR (100.5 MHz, $CDCl_3$): $\delta = 162.42$, 162.03 (*C*=O), 156.09 (C_{aromat}), 149.78, 149.53 (α-*C*), 144.43, 144.30, 144.16, 144.04, 144.01, 143.88, 143.83, 143.81, 143.78, 143.74, 143.71, 143.60, 143.36, 143.16, 143.05, 142.90, 142.46, 142.39, 141.86, 141.82, 141.55, 141.50, 141.28, 140.98, 140.79, 140.48, 140.40, 139.61, 139.57, 138.81, 137.47 (C_{60} sp^2-*C*/C_{aromat}), 134.18, 134.14 (*C*H$_{aromat}$), 131.82, 131.78, 131.75, 131.70 (β-*C*H), 129.68, 127.85, 127.47, 127.27, 127.18, 127.14, 126.26 (*C*H$_{aromat}$), 122.05 (*meso-C*), 120.92 (*C*H$_{aromat}$), 120.81, 119.89 (*meso-C*), 113.83 (*C*H$_{aromat}$), 70.54 (C_{60} sp^3-*C*), 66.18, 64.57 (*C*H$_2$), 53.09 (O*C*H$_3$), 51.11 ppm (cyclopropan-*C*); UV/Vis (CH_2Cl_2): λ_{max} ($\log\varepsilon$) = 257 (5.15), 328 (4.73), 401 (sh, 4.60), 427 (5.44), 551 (4.29), 588 nm (3.84); MS (FAB): *m/z*: 1557 $[M+H]^+$; FT-IR (KBr): $\tilde{\nu} =$ 3049, 3022, 2988, 2923, 1748, 1596, 1438, 1339, 1232, 1003, 796, 700, 526 cm^{-1}.

The correct structural assignment of the *trans*-2 addition pattern carried out in reference [18b] was further corroborated: 1) The dyad was hydrolyzed according to reference [44] to give the corresponding bis-malonic acid derivative. According to the same procedure the known bis-adducts *trans*-2-C_{62}(COOEt)$_4$ and *trans*-3-C_{62}(COOEt)$_4$[18f] were hydrolyzed to give the bis-malonic acid derivatives *trans*-2-C_{62}(COOH)$_4$ and *trans*-3-C_{62}(COOH)$_4$. The comparison with the corresponding *trans*-3 derivative was carried out because this is the only other possible C_2-symmetric *trans* addition pattern and the C_2-symmetry within the dyad is unambiguously proven. After hydrolysis of the Zn dyad *trans*-2-C_{62}(COOH)$_4$ and not *trans*-3-C_{62}(COOH)$_4$ was formed as demonstrated by the dentity of the HPLC retention times: k' (HPLC, SiO_2, methanol, flow rate 1.4 mL min^{-1}) = 1.47 and the electronic absorption spectra (e.g., characteristic *trans*-2 absorption at 435 nm). 2) Molecular Modeling: To account for the flexibility of the alkyl chains within the free base model dyads with *trans*-2 and *trans*-3 addition patterns, MD simulations at 300 K for a simulation time of 10 ps (time step 0.001 ps) have been performed. For each adduct five independent simulations were carried out and the corresponding equilibrium structures were used as starting geometries for energy minimization at 0 K optimization using the MM$^+$ force field. The free bases were chosen as models because parameters for zinc are not unavailable within this force field, MM$^+$. The averaged energies computed thereafter were used to compare the stabilities of the *trans*-2 and *trans*-3 derivatives. The energy data clearly show that *trans*-2 isomer (HOF = 668.6 kcal M^{-1}) is much more stable than *trans*-3 isomer (HOF = 861.9 kcal M^{-1}).

Acknowledgement

This work was supported by the Stiftung Volkswagenwerk, the European Community (HPRNT-CT-2002–00177 program WONDERFULL), SFB 583 (Redoxaktive Metallkomplexe Reaktivitätssteuerung durch molekulare Architekturen), the Office of Basic Energy Sciences of the US Department of Energy and MIUR (cofin 2002, prot. 2002032171). This is contribution NDRL-4477 of the Radiation Laboratory.

[1] a) F. L. Carter, *Molecular Electronic Devices*, Dekker, New York, **1987**; b) *Photoinduced Electron Transfer* (Eds.: M. A.Fox, M. Channon), Elsevier, Amsterdam, **1988**; c) *Electron Transfer in Chemistry* (Ed.: V. Balzani), Wiley-VCH, Weinheim, **2001**.

[2] a) M. D. Newton, *Chem. Rev.* **1991**, *91*, 767; b) M. R. Wasielewski, *Chem. Rev*. **1992**, *92*, 435; c) D. Gust, T. A. Moore, A. L. Moore, *Acc. Chem. Res.* **1993**, *26*, 198; d) M. N. Paddon-Row, *Acc. Chem. Res.* **1994**, *27*, 18; e) I. R. Gould, S. Farid, *Acc. Chem. Res.* **1996**, *29*, 522; f) V. Balzani, A. Juris, M. Venturi, S. Campagna, S. Serroni, *Chem. Rev.* **1996**, *96*, 759; g) I. Willner, *Acc. Chem. Res.* ***1997***, *30*, 347; h) P. Piotrowiak, *Chem. Soc. Rev*. **1999**, *28*, 143; i) H. Kurreck, M. Huber, *Angew. Chem*. **1995**, *107*, 929; *Angew. Chem. Int. Ed. Engl.* **1995**, *34*, 849.

[3] Leading examples of noncovalent donor acceptor assemblies: a) P. Tecilla, R. P. Dixon, G. Slobodkin, D. S. Alavi, D. H. Waldeck, A. D. Hamilton, *J. Am. Chem. Soc.* **1990**, *112*, 9408; b) P. J. F. de Rege, S. A. Williams, M. J. Therien, *Science* **1995**, *269*, 1409; c) J. P. Kirby, J. A. Roberts, D. G. Nocera, *J. Am. Chem. Soc.* **1997**, *119*, 9230; d) S. L. Springs, D. Gosztola, M. R. Wasielewski, V. Kral, A. Andrievsky, J. L. Sessler, *J. Am. Chem. Soc.* **1999**, *121*, 2281; e) K. Yamada, I. Imahori, E. Yoshizawa, D. Gosztola, M. R. Wasielewski, Y. Sakata, *Chem. Lett.* **1999**, 235; f) M.-J. Blanco, M. C. Jimenez, J.-C. Chambron, V. Heitz, M. Linke, J.-P. Sauvage, *Chem. Soc. Rev.* **1999**, *28*, 293; g) J. L. Sessler, B. Wang, S. L. Springs, C. T. Brown, *Compr. Supramol. Chem.* Oxford, **1996**, *4*, 311.

[4] *The Photosynthetic Reaction Center* (Eds.: J. Deisenhofer, J. R. Norris), Academic Press, San Diego, **1993**.

[5] a) H. Imahori, Y. Sakata, *Adv. Mater.* **1997**, *9*, 537; b) M. Prato, *J. Mater. Chem*. **1997**, *7*, 1097. c) N. Martín, L. Sánchez, B. Illescas, I. Pérez, *Chem. Rev*. **1998**, *98*, 2527; d) F. Diederich, M. Gomez-Lopez, *Chem. Soc. Rev*. **1999**, *28*, 263; e) H. Imahori, Y. Sakata, *Eur. J. Org. Chem*. **1999**, 2445. f) D. M. Guldi, *Chem. Commun*. **2000**, 321; f) D. Gust, T. A. Moore, A. L. Moore, *Acc. Chem. Res.* **2001**, *34*, 40.

[6] Leading examples: a) H. Imahori, K. Hagiwara, M. Aoki, T. Akiyama, S. Taniguchi, T. Okada, M. Shirakawa, Y. Sakata, *J. Am. Chem. Soc*. **1996**, *118*, 11771; b) S. Fukuzumi, K. Ohkubo, H. Imahori, J. Shao, Z. Ou, G. Zheng, Y. Chen, R. K. Pandey, M. Fujitsuka, O. Ito, K. M. Kadish, *J. Am. Chem. Soc*. **2001**, *123*, 10676.

[7] Leading examples: a) P. A. Liddell, D. Kuciauskas, J. P. Sumida, B. Nash, D. Nguyen, A. L. Moore, T. A. Moore, D. Gust, *J. Am. Chem. Soc*. **1997**, *119*, 1400; b) D. Kuciauskas, P. A. Liddell, S. Lin, T. E. Johnson, S. J. Weghorn, J. S. Lindsey, A. L. Moore, T. A. Moore, D. Gust, *J. Am. Chem. Soc*. **1999**, *121*, 8604.

[8] Leading examples: a) N. Armaroli, F. Diederich, C. O. Dietrich-Buchecker, L. Flamigni, G. Marconi, J.-F. Nierengarten, J.-P. Sauvage, *Chem. Eur. J.* **1998**, *4*, 406; b) J.-F. Nierengarten, C. Schall, J.-F. Nicoud, *Angew. Chem.* **1998**, *110*, 2037; *Angew. Chem. Int. Ed.* **1998**, *37*, 1934.

[9] Leading examples: a) P. S. Baran, R. R. Monaco, A. U. Khan, D. I. Schuster, S. R. Wilson, *J. Am. Chem. Soc*. **1997**, *119*, 8363; b) D. I. Schuster, P. Cheng, S. R. Wilson, V. Prokhorenko, M. Katterle, A. R. Holzwarth, S. E. Braslavsky, G. Klihm, R. M. Williams, C. Luo, *J. Am. Chem. Soc.* **1999**, *121*, 11599

[10] Leading examples: a) N. V. Tkachenko, L. Rantala, A. Y. Tauber, J. Helaja, P. H. Hynninen, H. Lemmetyinen, *J. Am. Chem. Soc.* **1999**, *121*, 9378; b) N. V. Tkachenko, E. Vuorimaa, T. Kesti, A. S. Alekseev, A. Y. Tauber,; P. H. Hynninen, H. Lemmetyinen, *J. Phys. Chem. B* **2000**, *104*, 6371.

[11] Leading examples: a) M. J. Shephard, M. N. Paddon-Row, *Aust. J. Chem*. **1996**, *49*, 395; b) T. D. M. Bell, T. A. Smith, K. P. Ghiggino, M. G. Ranasinghe, M. J. Shephard, M. N. Paddon-Row, *Chem. Phys. Lett.* **1997**, *268*, 223.

[12] Leading example: a) F.-P. Montforts, O. Kutzki, *Angew. Chem.* **2000**, *112*, 612; *Angew. Chem. Int. Ed.* **2000**, *39*, 599.

[13] Leading examples: a) F. D'Souza, G. R. Deviprasad, M. S. Rahman, J.-P. Choi, *Inorg. Chem.* **1999**, *38*, 2157; b) F. D'Souza, G. R. Deviprasad, M. E. El-Khouly, M. Fujitsuka, O. Ito, *J. Am. Chem. Soc*. **2001**, *123*, 5277.

[14] L. Echegoyen, L. E. Echegoyen, *Acc. Chem. Res.* **1998**, *31*, 593.

[15] a) M. Prato, M. Maggini, *Acc. Chem. Res.* **1998**, *31*, 519; b) F. Diederich, R. Kessinger, *Acc. Chem. Res.* **1999**, *32*, 537; c) "Fullerenes and Related Structures": *Top. Curr. Chem.* **1999**, *199*, whole volume; d) *Lecture Notes on Fullerene Chemistry*, (Ed.: R. Taylor), Imperial College Press, London, **1999**; e) S. R. Wilson, D. I. Schuster, B. Nuber, M. S. Meier, M. Maggini, M. Prato, R. Taylor, in *Fullerene, Chemistry, Physics and Technology* (Eds.: K. M. Kadish, R. S. Ruoff), Wiley, New York, **2000**.

[16] a) H. Imahori, K. Hagiwara, T. Akiyama, M. Aoki, S. Taniguchi, T. Okada, M. Shirakawa, Y. Sakata, *Chem. Phys. Lett*. **1996**, *263*, 545; b) D. M. Guldi, K.-D. Asmus, *J. Am. Chem. Soc*. **1997**, *119*, 5744; c) D. M. Guldi, M. Prato, *Acc. Chem. Res.* **2000**, *33*, 695.

[17] For orientation effects: a) J. L. Sessler, M. R. Johnson, T.-Y. Lin, S. E. Creager, *J. Am. Chem. Soc.* **1988**, *110*, 3659; b) Y. Sakata, S. Nakashima, Y. Goto, T. Asahi, M. Hagihara, S. Nishikawa, T. Okada, N. Mataga, *J. Am. Chem. Soc.* **1989**, *111*, 8979; c) A. M. Brun, A. Harriman, V. Heitz, J.-P. Sauvage, *J. Am. Chem. Soc.* **1991**, *113*, 8657; d) A. Helms, D. Heiler, G. McLendon, *J. Am. Chem. Soc.* **1991**, *113*, 4325; e) H. A. Staab, S. Nikolic, C. Krieger, *Eur. J. Org. Chem.* **1999**, 1459; f) I. Read, A. Napper, R. Kaplan, M. B. Zimmt, D. H. Waldeck, *J. Am. Chem. Soc.* **1999**, *121*, 10976; g) R. W. Kaplan, A. M. Napper, D. H. Waldeck, M. B. Zimmt, *J. Am. Chem. Soc.* **2000**, *122*, 12039; h) N. R. Lokan, M. N. Paddon-Row, M. Koeberg, J. W. Verhoeven, *J. Am. Chem. Soc.* **2000**, 122, 5075; i) T. D. M. Bell, K. A. Jolliffe, K. P. Ghiggino, A. M. Oliver, M. J. Shephard, S. J. Langford, M. N. Paddon-Row, *J. Am. Chem. Soc.* **2000**, *122*, 10661; j) A. Ambroise, R. W. Wagner, P. D. Rao, J. A. Riggs, P. Hascoat, J. R. Diers, J. Seth, R. K. Lammi, D. F. Bocian, D. Holten, J. S. Lindsey, *Chem. Mater.* **2001**, *13*, 1023; k) M. Goes, M. de Groot, M. Koeberg, J. W. Verhoeven, N. R. Lokan, M. J. Shephard, M. N. Paddon-Row, *J. Phys. Chem. A* **2002**, *106*, 2129.

[18] a) E. Dietel, A. Hirsch, J. Zhou, A. Rieker, *J. Chem. Soc. Perkin Trans. 2* **1998**, 1357; b) E. Dietel, A. Hirsch, E. Eichborn, A. Rieker, S. Hackbarth, B. Röder, *Chem. Commun*. **1998**, 1981. c) D. M. Guldi, C. Luo, M. Prato, E. Dietel, A. Hirsch, *Chem. Commun.* **2000**, 373; d) D. M. Guldi, C. Luo, M. Prato, A. Troisi, F. Zerbetto, M. Scheloske, E. Dietel, W. Bauer, A. Hirsch, *J. Am. Chem. Soc.* **2001**, *123*, 9166; e) X. Camps, E. Dietel, A. Hirsch, S. Pyo, L. Echegoyen, S. Hackbarth, B. Röder, *Chem. Eur. J.* **1999**, *5*, 2362; f) A. Hirsch, I. Lamparth, H. R. Karfunkel, *Angew. Chem*. **1994**, *106*, 453; *Angew. Chem. Int. Ed. Engl.* **1994**, *33*, 437; g) A. Hirsch, I. Lamparth, T. Groesser, H. R. Karfunkel, *J. Am. Chem. Soc.* **1994**, *116*, 9385; h) A. Herzog, A. Hirsch, O. Vostrowsky, *Eur. J. Org. Chem.* **2000**, 171; i) A. Hirsch, O. Vostrowsky, *Eur. J. Org. Chem.* **2001**, 829.

[19] J. S. Lindsey, I. C. Schreiman, H. C. Hsu, P. C. Kearney, A. M. Marguerettaz, *J. Org. Chem*. **1987**, *52*, 827.

[20] For the synthesis and photophysical investigations of similiar dyads inlcuding those with a *trans*-1 addition pattern see: J.-P. Bourgois, F. Diederich, L. Echegoyen, J.-F. Nierengarten, *Helv. Chim. Acta* **1998**, *81*, 1835.

[21] For leading references on tether directed bisfunctionalization of C_{60} see: a) J.-F. Nierengarten, T. Habicher, R. Kessinger, F. Cardullo, F. Diederich, V. Gramlich, J. P. Gisselbrecht, C. Boudon, M. Gross, *Helv. Chim. Acta* **1997**, *80*, 2238; b) U. Reuther, T. Brandmüller, W. Donaubauer, F. Hampel, A. Hirsch, *Chem. Eur. J.* **2002**, *8*, 2261.

[22] HYPERCHEM, Hypercubes, http://www.hyper.com; Heating time: 10 ps, run time 15 ps, cooling time: 50 ps; starting temperature 0 °K, simulation temperature: 1200 °K, final temperature: 0 °K. For references see: a) W. F. van Gusteren, H. J. C. Berendsen, *Angew. Chem.* **1990**, *102*, 1020; *Angew. Chem. Int. Ed. Engl.* **1990**, *29*, 992; b) G. H. Grant, W. G. Richards, *Computional Chemistry*, Oxford University Press **1955**, p. 51; c) J. Helaja, A. Y. Tauber, Y. Abel, N. V. Tkachenko, H. Lemmetyinen, I. Kipelainen, P. H. Hynninen, *J. Chem. Soc. Perkin*

Trans. 1 **1999**, *16*, 2403; d) P. Bonnet, C. Jaime, L. Morin-Allory, *J. Org. Chem.* **2001**, *66*, 689.

[23] a) M. M. Olmstead, D. A. Costa, K. Maitra, B. C. Noll, S. L. Phillips, P. M. van Calcar, A. L. Balch, *J. Am. Chem. Soc*. **1999**, *121*, 7090; b) P. D. W. Boyd, M. C. Hodgson, C. E. F. Rickard, A. G. Oliver, L. Chaker, P. J. Brothers, R. D. Bolskar, F. S. Tham, C. A. Reed, *J. Am. Chem. Soc*. **1999**, *121*, 10487; c) D. V. Konarev, I. S. Neretin, Y. L. Slovokhotov, E. I. Yudanova, N. V. Drichko, Y. M. Shul′ga, B. P. Tarasov, L. L. Gumanov, A. S. Batsanov, J. A. K. Howard, R. N. Lyubovskaya, *Chem. Eur. J.* **2001**, *7*, 2605.

[24] D. M. Guldi, K.-D. Asmus, *J. Phys. Chem. A* **1997**, *101*, 1472.

[25] N. Armaroli, G. Marconi, L. Echegoyen, J.-P.Bourgeois, F. Diederich, *Chem. Eur. J.* **2000**, *6*, 1629.

[26] The excitation spectrum of the $\mathbf{C_{60}}$ emission is an exact match of the **ZnP** excitation spectrum and the **ZnP** ground state features (i.e., Q-bands).

[27] T. Förster, *Discuss. Faraday Soc.* **1959**, *27*, 7; the overlap integral ($J = 2.3 \times 10^{-14}\ \mathrm{cm^6\,mol^{-1}}$) was evaluated on the basis of Equation (6). For calculations of the critical distance R_c [Eq. (7)], K^2 the geometry factor was chosen as 2/3, N the Avogardo constant as $6.022 \times 10^{23}\ \mathrm{mol^{-1}}$ and n as the refractive index of the solvent.

$$J = \frac{\int [F(\tilde{\nu})\varepsilon(\tilde{\nu})]/\tilde{\nu}^4\, \mathrm{d}\tilde{\nu}}{\int F(\tilde{\nu})\mathrm{d}\tilde{\nu}} \quad (6)$$

$$R_c^6 = \frac{9000(\ln 10)K^2\Phi}{128\pi^5 N n^4} J \quad (7)$$

[28] D. L. Dexter, *J. Chem. Phys.* **1953**, *21*, 836 The overlap integral ($J = 5.0 \times 10^{-4}\ \mathrm{cm^{-1}}$) was evaluated on the basis of Equation (8):

$$J = \frac{\int F(\tilde{\nu})\varepsilon(\tilde{\nu})\, \mathrm{d}\tilde{\nu}}{\int F(\tilde{\nu})\, \mathrm{d}\tilde{\nu} \int \varepsilon(\tilde{\nu})\, \mathrm{d}\tilde{\nu}} \quad (8)$$

[29] The CT emission is found upon excitation into 1) the fullerene features (i.e., 325 nm), 2) the porphyrin features (i.e., 425 nm), and 3) the CT absorption (i.e., < 700 nm).

[30] a) H. Imahori, N. V. Tkachenko, V. Vehmanen, K. Tamaki, H. Lemmetyinen, Y. Sakata, S. Fukuzumi, *J. Phys. Chem. A* **2001**, *105*, 1750; b) V. Vehmanen, N. V. Tkachenko, H. Imahori, S. Fukuzumi, H. Lemmetyinen, *Spectrochim. Acta Part A* **2001**, *57*, 2229.

[31] S. Larsson, A. Klimkans, L. Rodriguez-Monge, G. Duskesas, *J. Mol. Struct.* **1998**, *425*, 155.

[32] Upon excitation of the fullerene core, for example, with a 355 nm laser pulse, CS also occurred with the exception of toluene. This confirms that both singlet states (^{1}***ZnP**: 2.00 eV; ^{1}***C$_{60}$**: 1.76 eV) are sufficiently energetic to power intramolecular CS processes.

[33] From Table 6, it appears that the quantum yields are largest for THF and dichloroethane.

[34] a) R. A. Marcus, N. Sutin, *Biochim. Biophys. Acta* **1985**, *811*, 265; b) R. A. Marcus, *Angew. Chem*. **1993**, *105*, 1161; *Angew. Chem. Int. Ed. Engl*. **1993**, *32*, 1111.

[35] $\lambda = 0.59$ eV and $V = 51\ \mathrm{cm^{-1}}$ (*meta*-**ZnP** – **C$_{60}$**).

[36] P. Vath, M. B. Zimmt, D. V. Matyushov, G. A. Voth, *J. Phys. Chem. B* **2000**, *103*, 9130.

[37] a) J. Ponder, F. Richards, *J. Comput. Chem*. **1987**, *8*, 1016; b) C. Kundrot, J. Ponder, F. Richards, *J. Comput. Chem.* **1991**, *12*, 402. c) M. J. Dudek, J. Ponder, *J. Comput. Chem*. **1995**, *16*, 791.

[38] a) N. L. Allinger, Y. H. Yuh, J.-H. Lii, *J. Am. Chem. Soc*. **1989**, *111*, 8551. b) J.-H. Lii, N. L. Allinger, *J. Am. Chem. Soc*. **1989**, *111*, 8566; c) J.-H. Lii, N. L. Allinger, *J. Am. Chem. Soc*. **1989**, *111*, 8576.

[39] a) D. A. Leigh, A. Murphy, J. P. Smart, M. S. Deleuze, F. Zerbetto, *J. Am. Chem. Soc.* **1998**, *120*, 6458; b) R. Caciuffo, A. Degli Esposti, M. S. Deleuze, D. A. Leigh, A. Murphy, B. Paci, S. Parker, F. Zerbetto, *J. Chem. Phys.* **1998**, *109*, 11094; c) M. S. Deleuze, D. A. Leigh, F. Zerbetto, *J. Am. Chem. Soc.* **1999**, *121*, 2364; d) V. Bermudez, N. Capron, G. Torsten, F. G. Gatti, F. Kajzar, D. A. Leigh, F. Zerbetto, S. Zhang, *Nature* **2000**, *406*, 608; e) M. Cavallini, M. R. Lazzaroni, R. Zamboni, F. Biscarini, D. Timpel, F. Zerbetto, G. J. Clarkson, D. A. Leigh, *J. Phys. Chem. B* **2001**, *10*, 10826.

[40] H. J. C. Berendsen, J. P. M. Postma, W. F. van Gunsteren, A. Di Nola, J. R. Haak, *J. Chem. Phys.* **1984**, *81*, 3684.

[41] H. C. Andersen, *J. Comput. Phys.* **1983**, *52*, 24.

[42] "Semi Empirical Molecular Orbital Methods": M. C. Zerner, *Rev. Comput. Chem.* **1999**, *2*, 313.

[43] a) G. Orlandi, A. Troisi, F. Zerbetto, *J. Am. Chem. Soc.* **1999**, *121*, 5392; b) A. Troisi, G. Orlandi *Chem. Phys. Lett.* **2001**, *344*, 509.

[44] I. Lamparth, A. Hirsch, *Chem. Commun.* **1994**, 1727.

Received: March 26, 2003 [F4995]

